

# We are IntechOpen, the world's leading publisher of Open Access books Built by scientists, for scientists

6,900

Open access books available

185,000

International authors and editors

200M

Downloads

Our authors are among the

154

Countries delivered to

TOP 1%

most cited scientists

12.2%

Contributors from top 500 universities



WEB OF SCIENCE™

Selection of our books indexed in the Book Citation Index  
in Web of Science™ Core Collection (BKCI)

Interested in publishing with us?  
Contact [book.department@intechopen.com](mailto:book.department@intechopen.com)

Numbers displayed above are based on latest data collected.  
For more information visit [www.intechopen.com](http://www.intechopen.com)



# Features of Volume Holograms in Fluoride and Chloride Photothermorefractive Glass

*Nikonorov Nikolay, Ivanov Sergei, Dubrovin Victor and Klyukin Dmitry*

## Abstract

Today, silicate photothermorefractive (PTR) glasses are well known as a holographic medium for fabrication of holographic volume diffractive optical elements. The photothermoinduced crystallization process is used for recording high-efficiency phase volume holograms in this material. These holograms are used for developing unique diffractive optical elements that provide new opportunities for the laser technique, for example, narrowband filters for solid-state lasers and laser diodes, beam combiners, holographic collimator sights, chirped gratings for laser pulse compression, etc. By now, the photothermoinduced crystallization and properties of the PTR glass are investigated well enough. However, there are some issues and features still, which are solved in the present work. The mechanism of refractive index change in fluoride photothermorefractive glass during photothermoinduced crystallization and refractive index profile of the volume Bragg gratings were discussed. We studied a fine structure of a core-shell system inside fluoride PTR glass in which a silver nanoparticle presents the core and crystalline phases of silver bromide and sodium fluoride present the shell. We report on the optical properties of volume Bragg gratings in chloride PTR glass after femtosecond laser bleaching. We demonstrated that the bleaching procedure significantly reduces the absorption and increases the thermal stability of the Bragg gratings.

**Keywords:** photothermorefractive glass, holography, Bragg grating, crystallization, bleaching

## 1. Introduction

Photothermorefractive (PTR) glasses are a new class of photosensitive materials intended for recording three-dimensional phase holograms. This glass originates from photosensitive sodium zinc aluminosilicate glasses that were applied by Stookey and Pierson in Corning, Inc. (USA) in 1977 for the first time and were referred to as polychromatic glass [1–4] worldwide and by Tsekhomsky in Vavilov State Optical Institute (Russia) [5, 6] as multichromatic (MC) glass. In the late 1980s to early 1990s [7–10], Glebov and Nikonorov in Vavilov State Optical Institute (Russia) were first proposed to implement MC glass for volume holography. This chapter is focused on the photothermoinduced crystallization process itself and the enhancement of the refractive index contrast between irradiated and nonirradiated

areas. As a result, a new class of materials was developed, which is denoted [10] by a specific term such as “photothermorefractive (PTR) glass” (i.e., glass wherein after UV irradiation and subsequent thermal treatment changes in refractive index occur). Later this term started to be used worldwide [11, 12].

Nowadays, there is an increased interest in the volume Bragg gratings recorded on PTR glass due to their outstanding properties. The main advantage of these glasses is their unique combination of working characteristics such as high spectral selectivity and operating angle, great mechanical and optical strength, and high chemical durability. A great number of optical elements have been developed based on PTR glass, including extra narrow-band filters, combiners of high-intensity light beams, wavelength division multiplexing (WDM) devices, filters for increasing the spectral brightness of laser diodes, chirped gratings for compressing the light impulses, etc.

By now, the photothermoinduced crystallization and properties of the PTR glass are investigated well enough. For example, the fluoride PTR glass was designed and synthesized in ITMO University, Russia [13]. It is a photosensitive multicomponent sodium-zinc-alumina-silicate glass containing fluorine (6 mol.%) and a small amount of bromine (0.5 mol.%). Also, the PTR glass is doped with cerium, antimony, and silver. These additives are responsible for the photothermoinduced crystallization process resulting in precipitation of silver nanoparticles and sodium fluoride crystals in the volume of the glass [2, 14, 15]. Untreated fluoride PTR glass is transparent in a wide spectral range of 250–2500 nm. The photothermoinduced crystallization process in the fluoride PTR glass consists of three stages: (i) a formation of neutral silver molecular clusters after UV irradiation into the  $\text{Ce}^{3+}$  absorption band, (ii) a formation of the silver nanoparticles under the subsequent heat treatment of the UV-irradiated PTR glass near the glass transition temperature ( $T_g$ ) [2], and (iii) a precipitation of silver bromide shells on the silver nanoparticles [16] and then a growth of sodium fluoride nanocrystals on them in shape of cones under the thermal treatment at temperatures above  $T_g$  [2, 17]. The basic optical and spectral properties of PTR glass are described in [2, 15, 18, 19].

In comparison with conventional holographic media (photopolymers, silver halides, gelatins, etc.), the fluoride PTR glass and the holographic optical elements (HOE)s recorded on the glass have outstanding operating characteristics. In particular, they demonstrate the high thermal stability of the HOEs and high resistance to the optical and ionizing irradiation. The optical and spectral parameters of the HOEs and gradient index (GRIN) elements do not change after its multiple heating to high enough temperature (500°C). HOEs recorded on the PTR glass show the high chemical stability and mechanical and optical resistance. From this point of view, the fluoride PTR glass reveals practically no difference with the commercial optical glass BK7 (Schott). The HOEs have a very high duration of life (dozens of years). The key advantages of fluoride PTR glass as a holographic medium are the following:

- i. high optical homogeneity (the refraction index fluctuations across the glass bulk are of the order of  $10^{-5}$ ),
- ii. high reproducibility of parameters of HOEs with high diffraction efficiency (above 99%),
- iii. variety of technologies of glass processing—the fluoride PTR glass (like commercial optical glass) can be subjected to various kinds of mechanical grinding and polishing and another shaping technology like pressing, molding, drawing fiber, as well as laser treatment, and ion exchange,

- iv. a simple synthesis of fluoride PTR glass allows us to fabricate the glass both in the laboratory conditions (hundreds of grams) and industrial ones (hundreds of kilograms). The chemical reagents required for glass fabrication are commercially available and not too expensive.

It should be noted that some features of fluoride PTR glass are unusual in comparison with other holographic media. The PTR glass contains sodium ions. These ions can be changed on another monovalent ion (silver, potassium, rubidium, and cesium) by a well-known ion-exchange technique. This approach allowed us to fabricate ion-exchanged optical, luminescent, and plasmonic waveguides as well as to increase the mechanical, thermal, and optical resistance of the glass [20].

In case of fluoride PTR glass, the photothermoinduced crystallization results in a negative change of the refractive index (RI) in the UV-irradiated area in comparison with that of the nonirradiated area ( $\Delta n = -1.0 \times 10^{-3}$ ). We managed to control the sign of the RI increment by changing the type of halide (fluoride to chloride) in the PTR glass composition. The substitution of fluorine by chlorine resulted in the precipitation of nanocrystalline phases of mixed silver and sodium chlorides in glass host after UV irradiation and thermal treatment, which leads to a positive RI changes  $\Delta n = +1.0 \times 10^{-3}$ . It should be noted that positive refractive index change in chloride PTR glass provides the opportunity not only for Bragg gratings but also for the optical waveguides recording.

Untreated chloride PTR glass has the same transparency as fluoride one. And the photothermoinduced crystallization process is similar to the fluoride glass. The first stage is a generation of molecular silver clusters during UV irradiation, and the second stage is a formation of silver nanoparticles under heat treatment. On the following third stage, the heat treatment of PTR glass at temperatures above  $T_g$  leads to the precipitation of silver nanoparticles with a shell consisting of mixed sodium and silver chlorides [19, 21]. The absorption coefficient of silver nanoparticles in chloride PTR glass (at 450 nm) is very high and exceeds  $100 \text{ cm}^{-1}$ . This huge absorption is a key disadvantage chloride PTR. Despite this, the chloride PTR glass exhibits a rather low level of scattering. This is due to the small sizes of silver nanoparticles (about 3 nm) and small size of silver and sodium chloride nanocrystals (less 27 nm) [19]. This fact allowed us to conclude that the chloride PTR glass is still very attractive recording medium for photonics applications and for HOEs.

Despite the photothermoinduced crystallization and properties of the PTR glass are investigated well enough, there are some issues still, which restrict a wide application of the PTR glass. This chapter is a survey of recent achievements of ITMO University (St. Petersburg, Russia) that are focused on the investigation of the following issues: (i) mechanism of refractive index change in fluoride PTR glass during photothermoinduced crystallization, (ii) refractive index profile of the volume Bragg gratings, (iii) fine structure of core-shell system inside fluoride PTR glass in which a silver nanoparticle presents the core and crystalline phases of silver bromide and sodium fluoride present the shell, (iv) bleach of volume Bragg gratings in chloride PTR glass for decreasing optical losses and improving their thermal stability.

## **2. Mechanism of refractive index change in fluoride PTR glass during photothermoinduced crystallization**

According to the calculations presented in [22], the residual stresses are the main reason of RIC in fluoride PTR glass. However, according to Nikonorov et al. [14], this effect is assumed to be due to the difference of refractive indexes of sodium fluoride nanocrystals and PTR glass. Recently, we conducted an experiment that proved

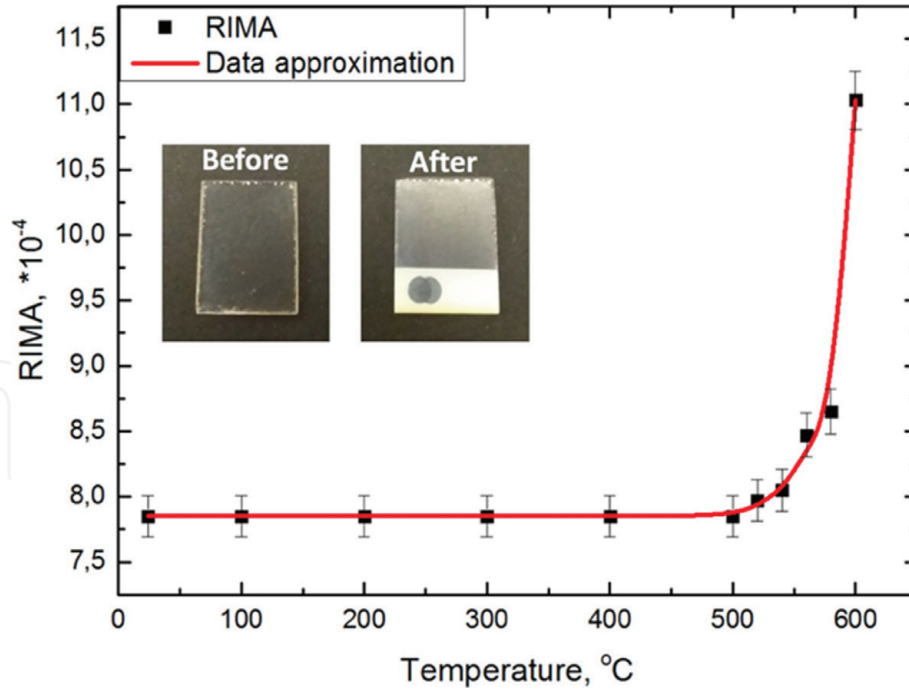


**Figure 1.**

*Refractive index modulation amplitude evolution depending on the sample temperature (photos of the sample before and after the experiment on the insert).*

that the origin of refractive index change in the PTR glass arises from the refractive index difference between PTR glass and NaF crystals.

In the experiment, transmission grating was heated in the chamber up to 600°C with 100°C step, while angular selectivity contour and diffraction efficiency (DE) were measured. Analysis of the selectivity contour revealed that heating up to the 500°C had no measurable effect on the grating DE and therefore on refractive index modulation amplitude (RIMA).

Also, it had been shown that DE of the grating starts to oscillate during the heating procedure as soon as the temperature reaches 480°C, which is due to the crystal growth process that begins around 480°C [21] and leads to RIMA value rapid increase with temperature (**Figure 1**).

Based on the results of our experiment, it is reasonable to conclude that the mechanical residual stresses cannot be the main reason of the RIC in PTR glass as even at 550°C, that is, 80°C higher than  $T_g$ , recorded Bragg grating is still functioning. Thus, the main reason for the refractive index contrast between exposed and unexposed areas is the refractive index difference between unperturbed glass and composite with NaF inclusions (**Figure 2**).

To estimate the RIC for this case, Maxwell Garnett theory [30] that allows to calculate the refractive index of the composite medium with the low volume fraction of inclusions had been applied.

To calculate the composite parameters, a model of needle NaF inclusions in the glass matrix had been chosen. In this case, the effective dielectric constant of the composite can be estimated according to the following equation [30]:

$$\delta = \left( \frac{\varepsilon - \varepsilon_h}{\varepsilon_i - \varepsilon_h} \right) \left( \frac{5\varepsilon_i + \varepsilon_h}{5\varepsilon + \varepsilon_h} \right)^{2/5} \quad (1)$$

where  $\delta$  is the NaF volume fraction,  $\varepsilon$  is the effective dielectric constant of a composite,  $\varepsilon_i$  is the dielectric constant of the NaF inclusions, and  $\varepsilon_h$  is the dielectric constant of the glass matrix.

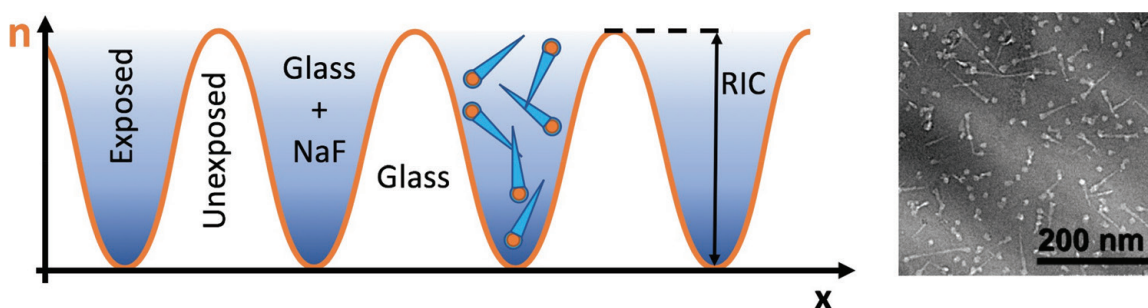


**Figure 2.**  
 Schematic representation of the volume Bragg grating (left) and TEM image of the actual grating fringe (right).

NaF volume fraction was calculated from the TEM image of the grating fringe (**Figure 2(right)**). Estimated difference of the refractive indices of such composite and unperturbed glass gave us  $27.62 \times 10^{-4}$ . It is clearly seen that this value is of the same order as the RIC in fluoride PTR glass after standard development procedure.

For experimental determination of RIC in the grating, five diffraction orders have been measured. Sum of all harmonics equals to the refractive index difference between exposed and unexposed areas and corresponds to  $27.92 \times 10^{-4}$ . At the same time, estimations based on Maxwell-Garnet theory gives us  $27.62 \times 10^{-4}$  that is close enough to the value obtained by the optical method. The difference between two methods can be attributed to rough approximations of the NaF crystal surrounding matrix refractive index as well as the fact that heat treatment leads to the changes in the refractive index of the unexposed glass [15].

Thus, it is shown that refractive index change in the exposed area appears primarily due to the NaF nanocrystal inclusions in the glass matrix, which according to the Maxwell-Garnet theory decreases the effective refractive index of such composite. It is shown experimentally that residual stresses have no measurable effect on the refractive index change.

### 3. Refractive index profile of the volume Bragg gratings

To record volume Bragg grating with holographic technique, one needs to interfere with two coherent beams inside the photosensitive medium. This interference will create a stationary wave with sinusoidal spatial profile of intensity. Next, a periodic variation of refractive index is inflicted by the process specific for each material. In our case, this process is used to be called photothermoinduced crystallization. Spatial distribution of the crystals results in a spatial modulation of the refractive index. In the case of nonsinusoidal gratings, refractive index profile can be expanded into a Fourier series where each harmonic represents the higher orders of diffraction. And of course, the more orders one sees, the less sinusoidal the gratings are. To utilize the whole refractive index change potential of the PTR glass, one needs to record pure sinusoidal gratings. We study the distribution of the RIC among the harmonics depending on the exposure dosage (**Figure 3(a)**).

As one can see, gratings with exposure of  $0.5 \text{ J/cm}^2$  have a nearly pure sinusoidal profile, 96.6% of RIC is in the first harmonic (**Figure 4**). It is expected that with an increase of exposure, fraction of the RIC in the first harmonic falls. However, it does not drop below 32% even when exposure doses are enormous like  $16 \text{ J/cm}^2$ .

It is reasonable to propose that the grating profile may be affected by the scattered light; however, in such case, fraction of the RIC at the first harmonic would fall with exposure linearly. However, **Figure 3(a)** represents the saturation effect. Thus, the fall of the first harmonic fraction is not related to the scattered light during the recording process.

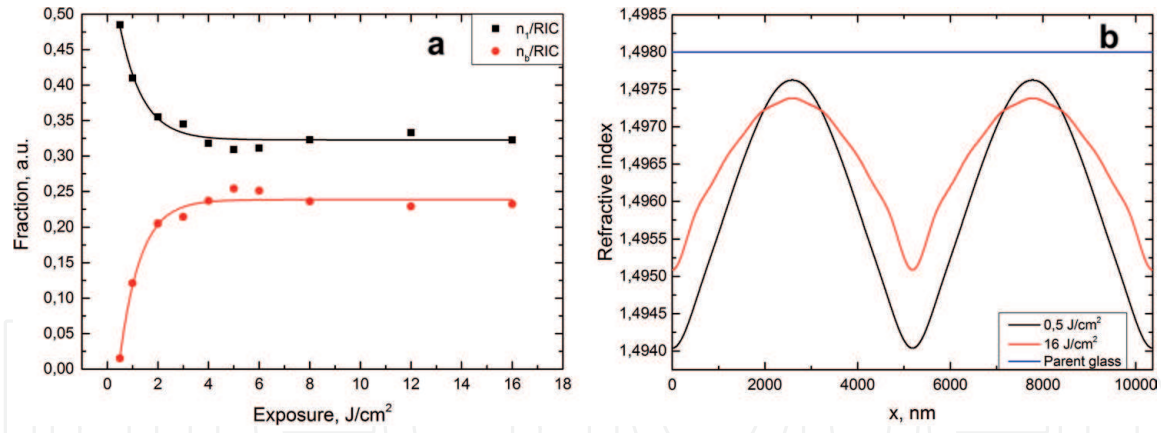


**Figure 3.** (a) Dependence of the RIC distribution between harmonics on dosage; (b) comparison of refractive index profile in the holographic grating with exposure 0.5 and 16 J/cm².

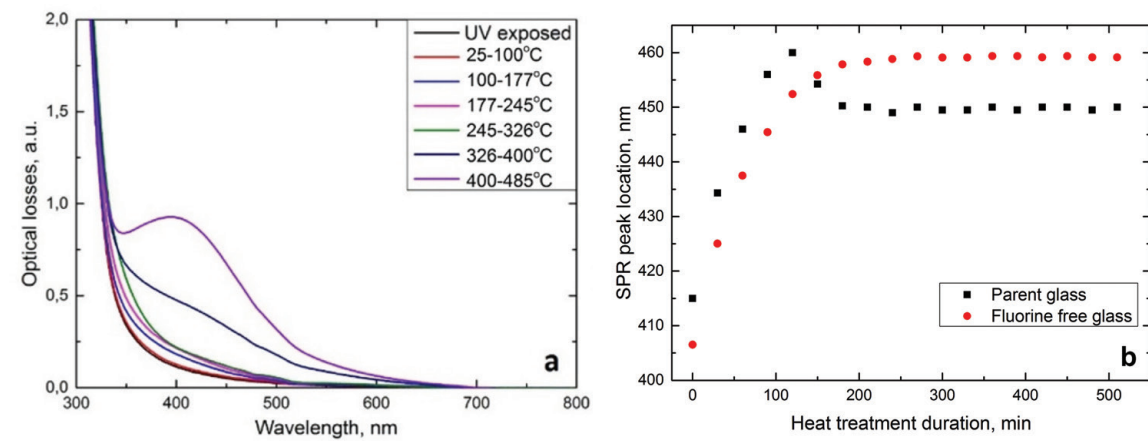


**Figure 4.** (a) Absorption spectrum dynamic of the UV irradiated and heated up to 485°C for 90 min fluoride PTR glass. (b) Dynamics of SPR peak location depending on the heat treatment duration for the parent PTR glass and glass with the lowest possible concentration of fluorine.

In [23], such effect was modeled considering the saturation of the RIC on exposure. Such saturation would lead to broadening of the grating fringes and decreasing the grating contrast. This situation can occur than in the interference pattern, maximum exposure already reached its saturation and thus does not contribute to further increase RIC. In this case, further exposure leads to a decrease in the contrast between the dark and the bright regions in terms of refractive index. However, our experiments show that fringes in the gratings with big exposure are narrower than that in gratings with small exposures **Figure 3(b)**. We suppose that the nonsinusoidal profile is a complex problem and cannot be explained with the saturation of exposure.

#### 4. Fine structure of core-shell system inside fluoride PTR glass

It is clear that (i) during photothermoinduced (PTI) crystallization process, the silver nanoparticles (NP) precipitate first (ii) that initiate sodium fluoride nanocrystals growth that is responsible for the refractive index changes. At the same time, the period between silver nanoparticles precipitation and sodium fluoride crystals growth is still unclear.

In **Figure 4(a)**, the evolution of the UV-irradiated fluoride PTR glass spectrum in the course of the heating process (heating up to 485°C for 90 min) is shown. It is seen clearly that until 300°C, no significant changes appear in the visible absorption

spectrum. Some processes occurring in this temperature range manifest themselves mostly in the UV. Such behavior had been discussed a lot in [18, 24] and attributed to the cerium and antimony ions in different valency. Further heating the sample leads to the formation of silver molecular clusters, thus causing an absorption increase in the visible. After it, when a temperature close to  $T_g$  is reached, it is seen that the SPR absorption peak corresponded to silver NPs manifesting in around 400 nm is already formed.

When starting the procedure of heat treating the sample, one can observe a significant redshift of the SPR peak location (**Figure 6**). Such behavior of the SPR band can be explained by the occurrence of the shell with a high refractive index on the silver nanoparticle.

During the photothermoinduced crystallization process of silver nanoparticles, precipitation occurs first, which is followed by formation of highly refractivity phase (silver bromide) when compared with glass matrix (1.498) [21]. It should be noted that after SPR peak location reaches 460 nm, it starts moving toward the shorter wavelengths up to 450 nm, and there, it remains independently from treatment duration time increase. The blueshift indicates the precipitation of NaF crystals that reduce the refractive index of the core-shell system surrounding. Stabilization of the peak location is due to the fact that NaF crystals already act as hosts for the core-shell structures. In the case of PTR glass without fluorine subjected to the same heat treatment procedure, the only redshift of the SPR resonance peak is observed (fluorine-free glass, **Figure 6(b)**). Hence, it can be concluded that the blue shift is inflicted by a decrease in the refractive index of the core-shell surrounding.

To estimate the size of silver nanoparticles, Lorenz-Mie scattering theory [8] was used.

The observed halfwidth of the plasmon resonance band at 415 nm equals to 100 nm that corresponds to the calculated average particle size of about 2.5 nm, which leads to the resonance wavelength of 407 nm. However, the SPR peak position of the parent glass heated up to the glass transition temperature is 415 nm (**Figure 4(b)**). This should mean that at this stage, NP is already in the shell.

Our simulation with silver bromide shell shows that several initial steps in the redshift cannot be achieved with this kind of crystal. A contrast in the refractive index between the silver bromide and the glass matrix is too high. Thus, we assumed that the refractive index of the shell is less than that of AgBr crystal.

On the other hand, initial SPR peak position (415 nm) can be modeled with 2.42 nm shell thickness of pure NaBr crystal. However, refractive index contrast between the NaBr crystal and PTR glass does not allow to achieve redshift of the SPR to the 460 nm. Considering these facts, we suppose that the shell should be of mixed composition. Whereby composition of the shell can be either a solid solution of NaBr and AgBr crystals or a glass-crystal composite where AgBr inclusions present in the glass matrix. These assumptions lead to a shell with a refractive index in the range of 1.68–2.25 depending on the AgBr fraction.

TEM image of the three-layer system (**Figure 5(a)**) provides us the outer diameter of the system, which can be roughly estimated to be 10 nm. This image was obtained from a sample with 460 nm SPR peak position. Thus, we conclude that 10 nm system diameter corresponds to the case where NaF is a host for a core-shell structure. Such a condition can be met only if the NaF layer thickness is above 3.17 nm. Considering the NP diameter of 2.5 nm, we adjudge that shell thickness equals to 0.57 nm (**Figure 5(b)**). It is a special mention that shell thickness correlates to the lattice constant of AgBr (0.597 nm) and NaBr (0.578 nm) crystals [23].

Since 0.57 nm is finite shell thickness, which already corresponds to the crystal lattice size, we will assume that the shell thickness is constant during the heat treatment procedure with the growing refractive index due to an increase in the AgBr concentration either in the solid solution or in the crystal-glass mixture.

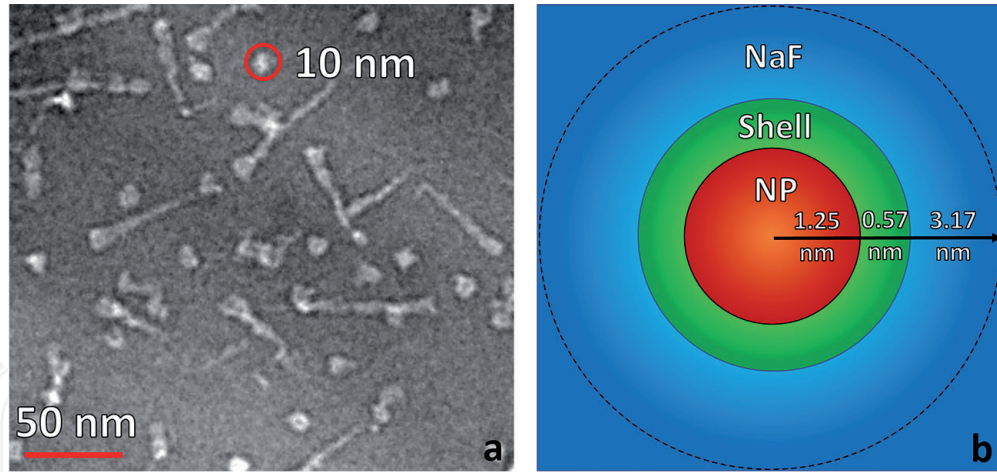


**Figure 5.** (a) TEM image of a grating fringe in conventional PTR glass and (b) three-layer system model according to our estimations and the TEM image of a real system.

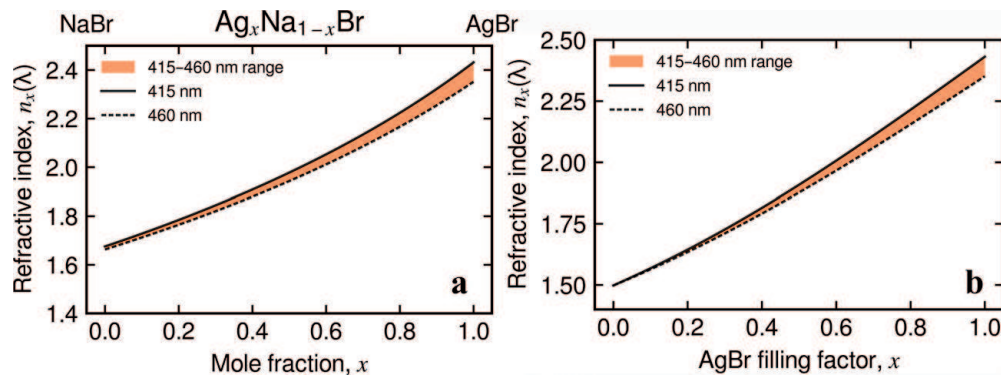


**Figure 6.** Estimated refractive index of the shell for solid solution (left) and Bruggeman (right) models.

The first approach implies that the shell of our three-layer system is a solid solution of AgBr and NaBr crystal where during the heat treatment procedure, concentration of the AgBr increases. Refractive index of this system was calculated according to Varotsos [25] and its variation can be seen from **Figure 6(a)**.

It can be seen from **Figure 6(a)** that initial SPR peak position at 415 nm corresponds to 1.8% AgBr concentration in the solid solution. Thus, according to this model, initial position of the SPR equals to almost pure NaBr shell (with respect to the accuracy of the measurement and deconvolution). On the other hand, the final peak position equals to the 88.7% of the AgBr in the solid solution; therefore, at the end of this process according to this model, shell still represents a solid solution of the two crystals.

According to the second approach, a constant layer of the glass around the silver NP is filling up with AgBr crystal cells during the heat treatment. Since the refractive index of AgBr is higher than that of the surrounding glass, this process leads to the effective refractive index increase of the layer. Refractive index of this layer can be estimated with Bruggeman's two-component effective model [26]. According to our calculation, SPR peak position of 415 nm corresponds to 25% of AgBr inclusion volume fraction (**Figure 6(b)**); on the other hand, that of 460 nm corresponds to 89% of inclusion. Thus, one can see that precipitation speed of AgBr on the NP decreases with the crystal concentration growth. Accepting this model leads to conclusions that (i) the precipitation of AgBr is the most rapid at the beginning of PTI crystallization process and (ii) there is a probability that, in the course of the NP formation, the silver bromide can already be present nearby.

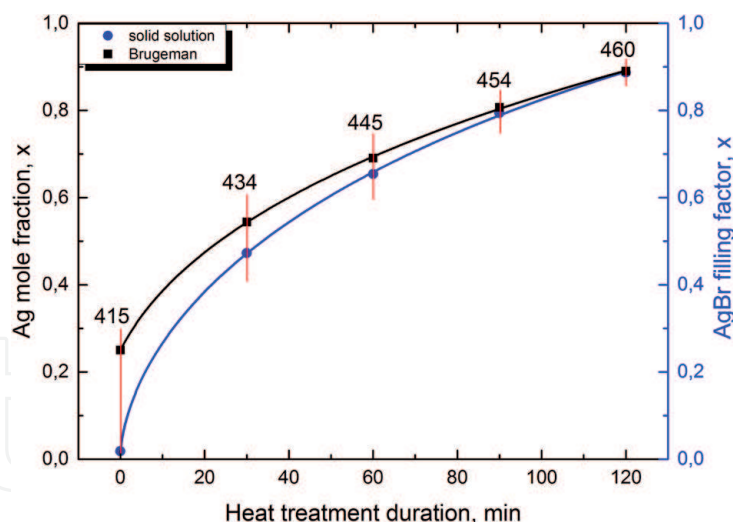


**Figure 7.** Evolution of Ag mole fraction and AgBr filling factor during the heat treatment process. The corresponding SPR peak positions are denoted in nm.

If we plot the concentration of AgBr in the shell as a function of the heat treatment duration for both above cases, the plots behave monotonically (**Figure 7**) and can be approximated with sigmoidal Weibull function with zero error. This means that both models demonstrate similar behavior with rapid growth at the beginning and severe speed decrease as the system is reaching its saturation (AgBr filling factor or mole fraction).

## 5. Bleaching volume Bragg gratings in chloride PTR glass

In comparison with fluoride PTR glass, the chloride ones provide positive refractive index change, very high induced absorption in visible spectral range, and small size of the crystalline phase that suppresses scattering and allows recording holograms with high spatial resolution. However, the diffraction efficiency of such amplitude-phase holograms is limited according to the coupled wave theory [27]. Therefore, absorption of sinusoidal VBGs is increased and causes a decline of diffraction efficiency [28]. Thus, high absorption in near IR and visible spectral range hinders this advantage and it is highly desirable to suppress absorption of such VBGs and leave only phase grating. Since the modulation of the absorption in the grating fringes originates from the strong surface plasmon resonance of silver nanoparticles (AgNPs), which can be reduced by bleaching (photodestruction process) of the AgNPs using femtosecond laser radiation.

**Figure 8** shows the optical density spectra of chloride PTR glass with recorded VBG before and after full femtosecond laser bleaching of the sample. It is seen that before the bleaching, glass possesses high absorption of surface plasmon resonance ( $>100 \text{ cm}^{-1}$ ) at 450 nm wavelength and visible spectral range. Inset to **Figure 9** shows the optical density spectrum of VBG after 10 hours of thermal treatment at 546°C when AgNPs concentration is fairly low. A dramatic decrease of optical density in visible can be observed after laser bleaching of the sample.

Two crystalline phases are precipitated in the volume of chloride PTR glass. The X-ray diffraction (XRD) analysis showed that the first phase is AgNPs, while the second phase is  $\text{Na}_{0.9}\text{Ag}_{0.1}\text{Cl}$  (NaCl-AgCl) nanocrystals. The XRD study was performed before and after laser bleaching. The XRD analysis demonstrated the photodestruction of AgNPs playing a role of the core on silver molecular clusters and ions and preservation of NaCl-AgCl nanocrystals in the form of a shell.

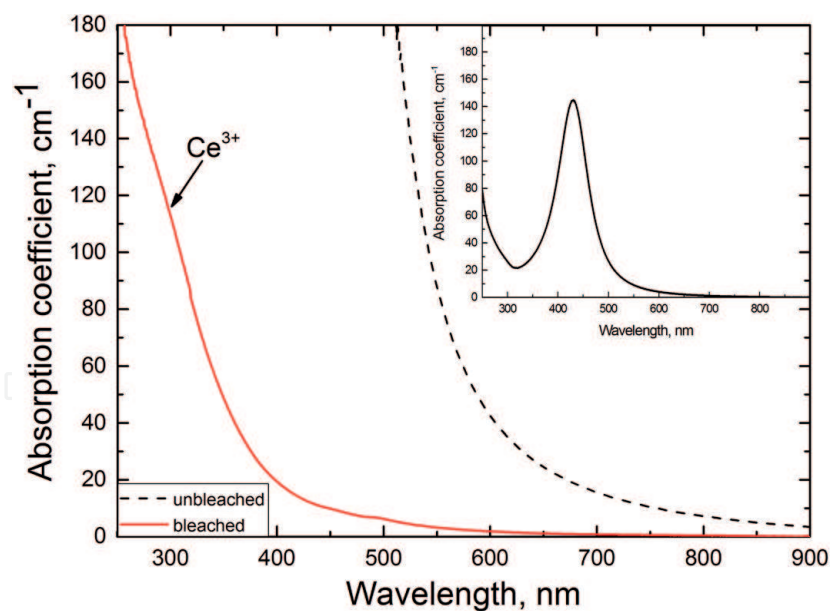


**Figure 8.** Absorption spectra of as-prepared PTR glass, VBGs before and after bleaching. Inset: optical density spectrum of VBG with small AgNPs concentration.

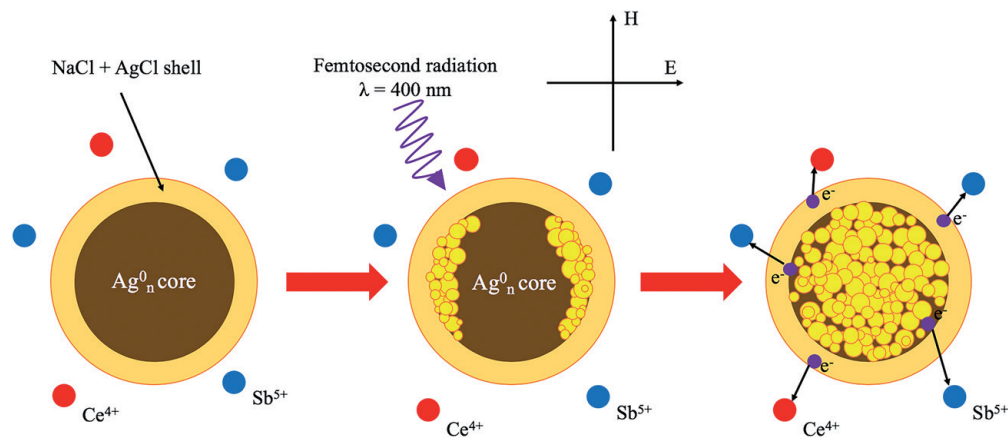


**Figure 9.** The mechanism for bleaching of AgNPs hologram.

The process of photodestruction of metallic nanoparticles is well known for different types of glass [29, 30]. The absorption of ultrashort pulse energy leads to local heating and the explosion of the metallic particle [31]. In **Figure 9**, process of AgNPs surrounded by NaCl-AgCl shell, destruction, is shown schematically [32]. The femtosecond bleaching transforms AgNPs into silver clusters. However, due to the presence of shell, the particle fragments cannot move far from the origin as available space is limited by the interior volume of NaCl-AgBr crystal. It should be noted that nanoparticle restoration time under thermal treatment takes several minutes that also indicates that silver clusters close to each other after bleaching.

Considering that the absorption caused by AgNPs plasmon resonance is not present at the spectrum of the grating, it was assumed that the grating becomes purely phase type after laser processing. Previously, it was shown that VBGs in chloride PTR glass are of a mixed type, that is, both refractive and absorption indexes are modulated in the glass volume [33]. In accordance with the coupled wave theory, the coupling constant ( $\chi$ ) responsible for the transfer of energy between the reference (R) and signal (S) wave contains refractive index modulation amplitude (RIMA) and absorption index modulation amplitude (AIMA). Hence, removal of the one causes a natural decline of the coupling efficiency as described by Collier [34].

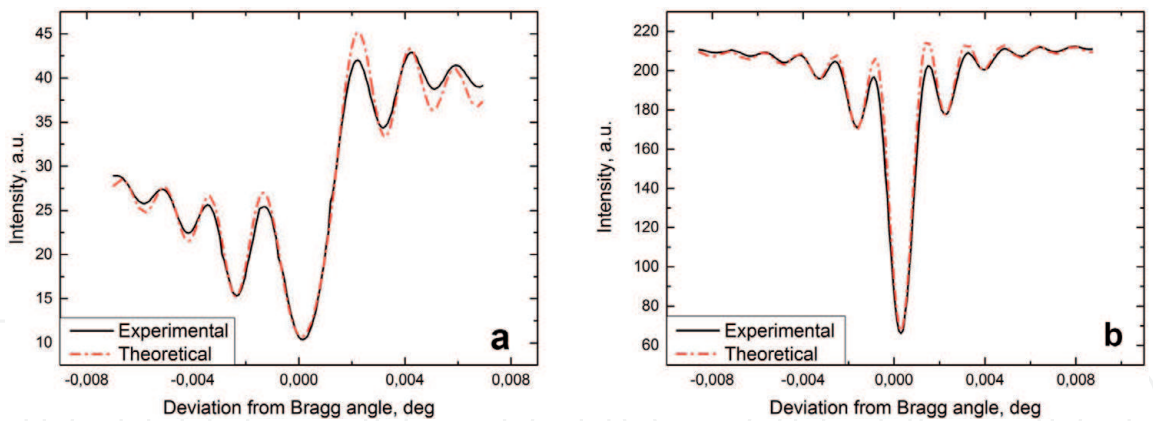


**Figure 10.** Experimental and fitted curves of angular selectivity contours before (a) and after (b) photodestruction of AgNPs in VBGs.

In order to characterize the contribution of RIMA and AIMA to the VBGs performance, one should analyze angular selectivity contour of zero diffraction order. It is critical as the first-order diffraction selectivity contour looks similar for both amplitude-phase and phase gratings with the same coupling.

Experimental and fitted angular selectivity contours for the holograms recorded in chloride PTR glass are shown in **Figure 10**. One can notice an asymmetric shape of the zeroth diffraction order contour before laser bleaching with respect to Bragg angle. It directly points out at mixed nature of the grating [28, 33, 35]. After laser processing, the contour becomes symmetric as shown in **Figure 10(b)**. These factors indicate the lack of absorption modulation in the hologram, so it became purely phase. Hence, the modification of the contour shape indicates a weakening of the coupling.

The further analysis consists of the estimation of the AIMA and RIMA [27, 28, 33, 35]. The calculation of these parameters can be carried out by the fitting of the contours obtained in the experiment with those predicted by the theory (**Figure 11**, red curves). The performed fitting of the experimental results allows one to evaluate RIMA magnitude for each grating in the exposure range of 1–12 J/cm<sup>2</sup> before and after bleaching (**Figure 11(a)**).

As it is shown in **Figure 11(a)** for the exposures above 6 J/cm<sup>2</sup>, the volume fraction of the crystalline phase and concentration of AgNPs saturated because RIMA value stopped increasing. Thus, all available silver and chlorine ions in the hologram fringe were utilized. Moreover, it should be noted that the RIMA values decreased after laser bleaching for all exposures and the magnitude of the change depends on the exposure.

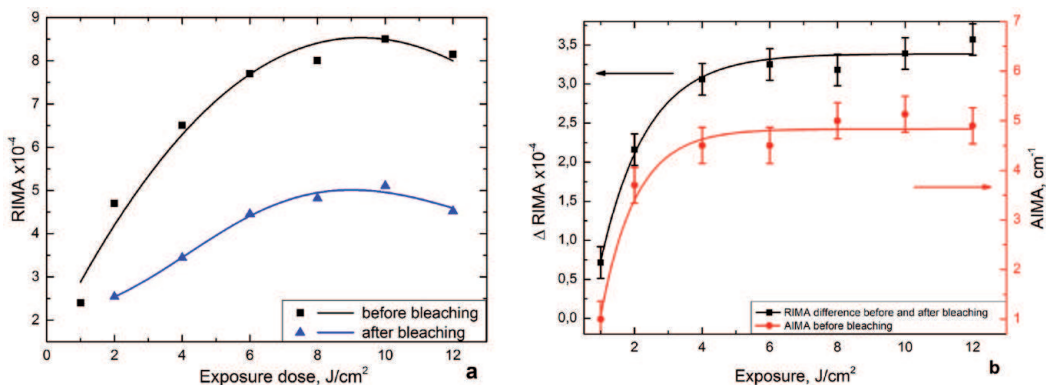


**Figure 11.** (a) RIMA before and after laser bleaching of VBGs. (b) Difference of RIMA before and after laser bleaching (curve with squares) and AIMA before laser bleaching (curve with circles).

The maximum value of RIMA was reduced from  $8.6 \times 10^{-4}$  down to  $5.1 \times 10^{-4}$ , that is, it became nearly two times lower after AgNPs photodestruction. As it is following from **Figure 11(b)**, the difference in the RIMA before and after laser processing and the AIMA vs. exposure demonstrates identical dependence on the exposure. It illustrates that additional RIMA, which was lost during the laser bleaching, was caused by the presence of the AgNPs in the hologram fringes and the value is correlated with their concentration. Although the dip of the RIMA value at the maximum is considerable, it was still sufficient to increase diffraction efficiency from 25 to 86%.

Thus, ultrashort laser bleaching of chloride PTR glass with VBGs causes a decline of RIMA from  $8.6 \times 10^{-4}$  to  $5.1 \times 10^{-4}$ , which is still adequate for efficient VBGs operation. After the laser processing, the hologram becomes purely phase modulated, so it is capable to reach high diffraction efficiency at specific exposure, thermal treatment, and appropriate grating thickness. The transmission range of the VBGs expanded dramatically in visible spectral range opening avenues toward using them for high-power laser applications. Additionally, the smaller size of nanocrystals coupled with the absence of absorption in the visible region boosts the performance of such holograms at the smaller grating periods.

## 6. Thermal stability of volume Bragg gratings in chloride PTR glass

As-prepared chloride PTR glass is transparent in whole visible and near IR spectral range until  $2.5 \mu\text{m}$ . The main drawback of chloride PTR glass is absorption in visible and near IR spectral range, caused by AgNPs possessing surface plasmon resonance (SPR) at 410–450 nm. Chloride PTR glass has high SPR absorption ( $>100 \text{ cm}^{-1}$ ) with considerable tail at near IR. In Section 5, we demonstrated that AgNPs absorption can be reduced using femtosecond laser radiation. Moreover, it was also demonstrated that AgNPs in chloride PTR glass can be bleached without photodestruction of NaCl-AgCl nanocrystals, responsible for refractive index modulation in VBGs. In this chapter, the bleaching effect on thermal stability of gratings recorded on chloride PTR glass is discussed. Such bleaching of chloride PTR glass with VBGs can open new opportunities for high-power laser diode (LD) applications in near-IR spectral range.

Absorption of gratings in chloride PTR glass at the wavelength of LD (972 nm) is  $1.8 \text{ cm}^{-1}$  before laser bleaching and  $0.05 \text{ cm}^{-1}$  after the bleaching. The latter corresponds to the absorption of as-prepared glass. It is clear that higher absorption of LD pumping light at wavelength 972 nm causes heat accumulation at VBG. Thus, at some point, the input power cannot be dissipated with a low thermal conductivity of the glass and the local temperature starts increasing. As following, the parameters of VBG such as refractive index difference, grating period, and absorption may change significantly.

For studying the thermal stability of VBGs, we measured the angular selectivity contour of transmission VBG at a wavelength of He-Ne laser before and after bleaching (**Figure 12**). Radiation of CW laser diode at wavelength 972 nm was used as a hitting source.

**Figure 12(a)** shows angular selectivity curves of VBG under different pumping of LD before femtosecond laser bleaching. A shift of Bragg wavelength under different pumping power indicates the increase of the grating period, which directly effects Bragg conditions for diffracted He-Ne laser beam. It is worth noting that the shape of the curve without laser diode irradiation is complex and contains two peaks, which indicates that the grating is overmodulated. The amplitude of central peak gradually decreases with the growth of the laser diode intensity. The actual amplitude drop is even more pronounced if one subtracts the background radiation, which can be observed far from the Bragg angle. So, it is reasonable to conclude that under high

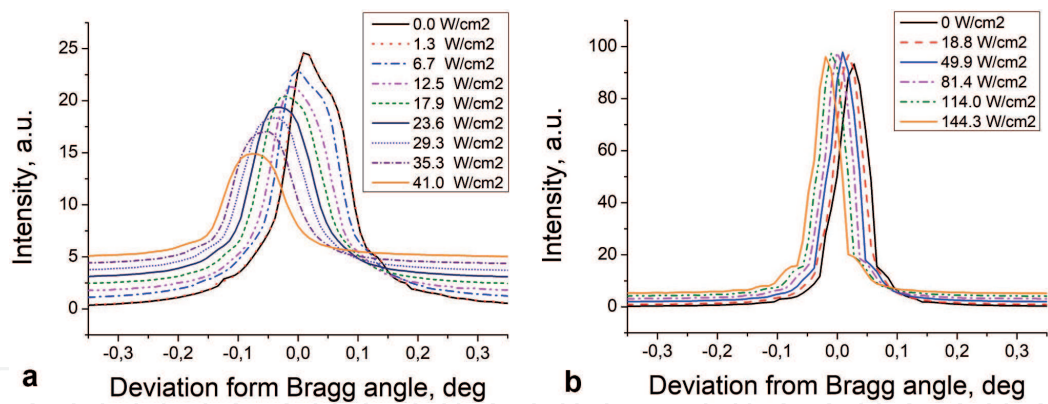


**Figure 12.**  
Angular selectivity at first order of diffraction of initial (a) and bleached (b) hologram.

power irradiation, the diffraction efficiency drops approximately by 30%. This result can be understood by taking into account the fact that at the beam intensity of 40 W/cm<sup>2</sup>, the grating temperature is about 350°C. It is known that the melting temperature of metal particle decreases for smaller particles. For AgNPs in silicate glass, melting temperature can be lower than 150°C, and optical properties of composite materials with embedded AgNPs change dramatically. The plasmon resonance absorption band of a liquid NP is broadening, which affects RIMA and AIMA values as it was discussed in the previous section. Melted AgNPs get crystallized back after cooling of the glass substrate with VBG and optical properties of the grating return to initial values.

**Figure 12(b)** shows angular selectivity contours after laser bleaching of VBGs under the different intensity of the LD diode beam. One can notice that the shift of the Bragg angle became smaller and the amplitude of the peak states unchanged even at higher fluence. The temperature increase in the irradiated area can be found from the following equation:

$$\Delta T = \frac{\Delta d}{d \cdot \alpha} \tag{2}$$

where  $d$  is a grating period,  $n$  is a refractive index of glass, and  $\alpha$  is a coefficient of thermal expansion. A grating temperature increase after laser bleaching at the level of 40°C for the same laser intensity is almost nine times smaller than before laser bleaching. **Figure 13** shows temperature increase and correspondent Bragg wavelength shift

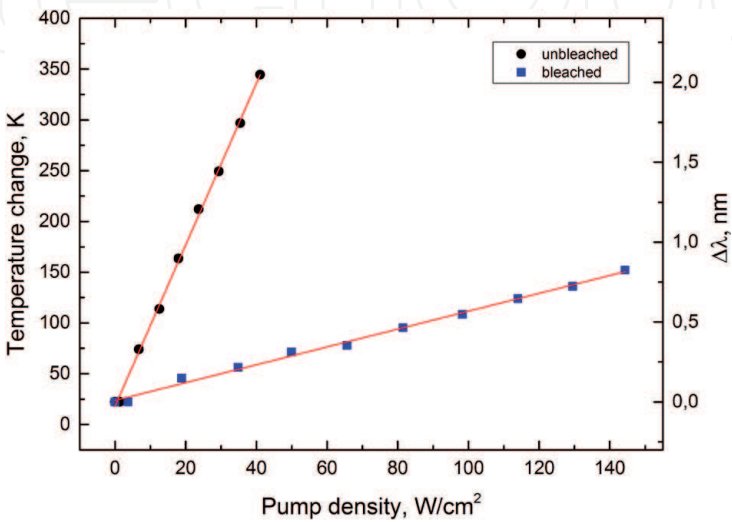


**Figure 13.**  
Dependence of temperature change and Bragg wavelength on the power density of the pumping source.

as functions of pump irradiance for VBGs before and after laser bleaching. A dramatic decrease in temperature after laser bleaching made it possible to increase pumping intensity almost four times from 40 to 145 W/cm<sup>2</sup>. In our experimental conditions, strong temperature gradients in the irradiated area resulted in the glass cracking when the pump intensity exceeds 145 W/cm<sup>2</sup>.

Thus, the bleaching technology can dramatically decrease heating of the grating under high power laser radiation, which enhances the stability of the grating's parameters such as period and RIMA.

## 7. Conclusions

Recent achievements of ITMO University (St. Petersburg, Russia) in the investigation of properties of holographic volume Bragg gratings in fluoride and chloride photothermorefractive glass are demonstrated. Some futures of the holograms are highlighted and discussed. Some ways of improvement of characteristics of the holograms are suggested.

Namely, the mechanism of refractive index change in fluoride photothermorefractive glass during photothermoinduced crystallization and refractive index profile of the volume Bragg gratings were discussed. It is shown that refractive index change in the exposed area appears primarily due to the NaF nanocrystal inclusions in the glass matrix, which according to the Maxwell-Garnet theory decreases the effective refractive index of such composite. It is shown experimentally that residual stresses have no effect on the refractive index change. Estimated refractive index difference between the composite and unperturbed glass is in a good agreement with the refractive index change obtained by the grating analysis.

The refractive index profile in the volume Bragg gratings on fluoride photothermorefractive glass was studied. It was shown that the nonsinusoidal profile of the gratings at high exposures cannot be explained by saturation of exposure since the fraction of the first harmonic stays the same at exposures above 6 J/cm<sup>2</sup>. In addition, it was shown that at higher exposures, grating fringes became narrower than that of the gratings with close to sinusoidal profile.

A fine structure of the core-shell system inside fluoride PTR glass in which a silver nanoparticle presents the core and crystalline phases of silver bromide and sodium fluoride present the shell was explored. In particular, for the three-layer system consisting of a silver nanoparticle, the bromide shell, and sodium fluoride shell, we made a numerical analysis of the peak location of surface plasmon resonance. The analysis showed that the thickness of the high refractive index shell does not exceed 0.5–0.6 nm. This result is in a good correlation with the unit cell size of the bromide crystals. We showed that the initial peak location of surface plasmon resonance cannot be explained by the formation of pure silver bromide shell or by the size of the silver nanoparticle. Moreover, the final peak location cannot be explained by the formation of sodium bromide shell alone. We demonstrated that the observed short-wavelength shift of the surface plasmon resonance peak at the later stage of photothermoinduced crystallization is due to the precipitation of sodium fluoride nanocrystals.

The optical properties of volume Bragg gratings in chloride PTR glass after femtosecond laser bleaching have been studied. The bleaching procedure significantly reduces the absorption of volume Bragg gratings (from 100 to 0.1 cm<sup>-1</sup>). Laser bleaching does not affect the amplitude of refractive index modulation of the grating. Femtosecond laser radiation breaks down silver nanoparticle to silver clusters and ions, but the NaCl-AgCl shell remains almost the same. Thus, the amplitude-phase grating is modified in the pure phase grating by femtosecond laser photodestruction of silver nanoparticles in the volume of PTR glass. Thus, the

increase of glass transmission in visible spectral range after laser bleaching of silver nanoparticles opens new opportunities for high laser power application.

It was shown that the bleaching procedure increases the thermal stability of the volume Bragg gratings under near IR laser diode pumping. So, the temperature change of the glass with volume Bragg grating under  $40 \text{ W/cm}^2$  power density has reduced from  $350$  to  $38^\circ\text{C}$ . The bleaching of volume gratings allowed us to reduce temperature drift of Bragg wavelength from  $50$  to  $6 \text{ pm/(W/cm}^2\text{)}$ . Thus, the bleaching technology can dramatically decrease heating of the grating under high power laser radiation, which enhances the stability of the grating parameters such as period and amplitude of refractive index modulation. It should be pointed out that the problem of silver nanoparticles absorption hinders not only chloride photothermorefractive glass because so far, all types of PTR glass (fluoride and bromide) also make use of silver nanoparticles precipitation for photothermoinduced crystallization. Thus, we believe that this approach can be utilized for bleaching of other types of PTR glass as well.

## Acknowledgements


This work was supported by the Ministry of Science and Higher Education of Russian Federation (Project 16.1651.2017/4.6).

## Author details

Nikonorov Nikolay\*, Ivanov Sergei, Dubrovin Victor and Klyukin Dmitry  
Saint-Petersburg National Research University of Information Technologies,  
Mechanics and Optics, St. Petersburg, Russian Federation

\*Address all correspondence to: [nikonorov@oi.ifmo.ru](mailto:nikonorov@oi.ifmo.ru)

## IntechOpen

© 2019 The Author(s). Licensee IntechOpen. This chapter is distributed under the terms of the Creative Commons Attribution License (<http://creativecommons.org/licenses/by/3.0>), which permits unrestricted use, distribution, and reproduction in any medium, provided the original work is properly cited. 

## References

- [1] Stookey SD. Photosensitive glass. Industrial & Engineering Chemistry Research. 1949;**41**(4):856-861
- [2] Stookey SD, Beall GH, Pierson JE. Full-color photosensitive glass. Journal of Applied Physics. 1978;**49**(10):5114
- [3] Pierson JE, Stookey SD. United States Patent 4,057,408; 1977
- [4] Pierson EJ, Stookey SD. United States Patent 4,017,318; 1977
- [5] Panysheva EI, Tunimanova IV, Tsekhomskii VA. A study of coloring in polychromatic glasses. Fizika i Khimiya Stekla. 1990;**16**(2):239-244. In Russian
- [6] Dotsenko AV, Efimov AM, Zakharov VK, Panysheva EI, Tunimanova IV. On the absorption spectra of polychromatic. Fizika i Khimiya Stekla. 1985;**11**(5):592-595. In Russian
- [7] Glebov LB, Nikonorov NV, Panysheva EI, Petrovskii GT, Savvin VV, Tunimanova IV, et al. New possibilities of photosensitive glasses for the recording of volume phase diagrams. Optika i Spektroskopiya. 1992;**73**(2):404-412. In Russian
- [8] Kuchinskii SA, Nikonorov NV, Panysheva EI, Savvin VV, Tunimanova I. Properties of volume phase holograms on polychromatic glasses. Optika i Spektroskopiya. 1991;**70**(6):1286-1300. In Russian
- [9] Nikonorov NV, Panysheva EI. Polychromatic glasses-a new medium for optical data recording. In: Opticheskoe Izobrazhenie i Registriruyushchie Sredy (All-Union Conference "Optical Image and Recording Media"). Leningrad: GOI; 1990. pp. 2-48. In Russian
- [10] Glebov LB, Nikonorov NV, Panysheva EI, Tunimanova IV, Savvin VV, Tsekhomskii VA. Photothermorefractive glass. In: IF AN Latv. SSR, editor. Trudy VII Vsesoyuznoi Konferentsii po Radiatsionnoi Fizike i Khimii Neorganicheskikh Materialov (Proceedings of VII All-Union Conference on Radiation Physics and Chemistry of Inorganic Materials); Riga. 1989. p. 527. In Russian
- [11] Efimov OM, Glebov LB, Glebova LN, Richardson KC, Smirnov VI. High efficiency Bragg gratings in photo-thermo-refractive glass. Applied Optics. 1999;**38**(2):619-627
- [12] Glebov LB, Glebova LN, Richardson KA, Smirnov VI. Photo-induced processes in photo-thermo-refractive glasses. In: Soc AC, editor. Proceedings of XV Congress on Glass. San Francisco; 1998
- [13] Ivanov SA, Ignat'ev AI, Nikonorov NV, Aseev VA. Holographic characteristics of a modified photothermorefractive glass. Journal of Optical Technology. 2014;**81**(6):356-360
- [14] Nikonorov NV, Panysheva EI, Tunimanova IV, Chukharev AV. Influence of glass composition on the refractive index change upon photothermo induced crystallization. Glass Physics and Chemistry. 2001;**27**(3):241-249. Available from: <http://link.springer.com/article/10.1023/A:1011392301107>
- [15] Glebova L, Lumeau J, Klimov M, Zanotto ED, Glebov LB. Role of bromine on the thermal and optical properties of photo-thermo-refractive glass. Journal of Non-Crystalline Solids. 2008;**354**(2-9):456-461. Available from: <http://linkinghub.elsevier.com/retrieve/pii/S0022309307010903>
- [16] Glebov LB, Nikonorov NV, Panysheva EI, Petrovskii GT, Savvin VV, Tunimanova IV, et al. New ways to use photosensitive glasses for recording volume phase holograms. Optics and Spectroscopy. 1992;**73**(2):237-241

- [17] Dyamant I, Abyzov AS, Fokin VM, Zanutto ED, Lumeau J, Glebova LN, et al. Crystal nucleation and growth kinetics of NaF in photo-thermo-refractive glass. *Journal of Non-Crystalline Solids*. 2013;**378**:115-120
- [18] Efimov AM, Ignatiev AI, Nikonorov NV, Postnikov ES. Quantitative UV-VIS spectroscopic studies of photo-thermo-refractive glasses. I. Intrinsic, bromine-related, and impurity-related UV absorption in photo-thermo-refractive glass matrices. *Journal of Non-Crystalline Solids*. 2011;**357**(19-20):3500-3512
- [19] Dubrovin VD, Ignatiev AI, Nikonorov NV. Chloride photo-thermo-refractive glasses. *Optical Materials Express*. 2016;**6**(5):1701. Available from: <https://www.osapublishing.org/abstract.cfm?URI=ome-6-5-1701>
- [20] Sgibnev YM, Nikonorov NV, Vasilev VN, Ignatiev AI. Optical gradient waveguides in photo-thermo-refractive glass formed by ion exchange method. *Journal of Lightwave Technology*. 2015;**33**(17):3730-3735
- [21] Nikonorov N, Ivanov S, Dubrovin V, Ignatiev A. New photo-thermo-refractive glasses for holographic optical elements: Properties and applications. In: Naydenova I, editor. *Holographic Materials and Optical Systems*. Dublin: InTech; 2017. pp. 435-461
- [22] Lumeau J, Glebova L, Golubkov V, Zanutto ED, Glebov LB. Origin of crystallization-induced refractive index changes in photo-thermo-refractive glass. *Optical Materials*. 2009;**32**(1):139-146
- [23] Lumeau J, Glebov LB. Effect of the refractive index change kinetics of photosensitive materials on the diffraction efficiency of reflecting Bragg gratings. *Applied Optics*. 2013;**52**(17):3993-3997
- [24] Efimov AM, Ignatiev AI, Nikonorov NV, Postnikov ES. Quantitative UV-VIS spectroscopic studies of photo-thermo-refractive glasses. II. Manifestations of  $Ce^{3+}$  and  $Ce(IV)$  valence states in the UV absorption spectrum of cerium-doped photo-thermo-refractive matrix glasses. *Journal of Non-Crystalline Solids*. 2013;**361**(1):26-37
- [25] Varotsos P. Determination of the dielectric constant of alkali halide mixed crystals. *Physica Status Solidi*. 1980;**100**(2):K133-K138
- [26] Bruggeman V DAG. Berechnung verschiedener physikalischer Konstanten von heterogenen Substanzen. I. Dielektrizitätskonstanten und Leitfähigkeiten der Mischkörper aus isotropen Substanzen. *Annalen der Physik*. 1935;**416**(7):636-664
- [27] Kogelnik H. Coupled wave theory for thick hologram gratings. *Bell System Technical Journal*. 1969;**48**(9):2909-2947
- [28] Carretero L, Madrigal RF, Fimia A, Blaya S, Beléndez A. Study of angular responses of mixed amplitude-phase holographic gratings: Shifted Borrmann effect. *Optics Letters*. 2001;**26**(11):786-788. Available from: <http://www.ncbi.nlm.nih.gov/pubmed/18040450>
- [29] Podlipensky AV, Grebenev V, Seifert G, Graener H. Ionization and photomodification of Ag nanoparticles in soda-lime glass by 150 fs laser irradiation: A luminescence study. *Journal of Luminescence*. 2004;**109**:135-142
- [30] Bigot J, Halte V, Merle J, Daunois A. Electron dynamics in metallic nanoparticles. *Chemical Physics*. 2000;**251**:181-203
- [31] Hashimoto S, Werner D, Uwada T. Studies on the interaction of pulsed lasers with plasmonic gold nanoparticles toward light manipulation, heat management, and nanofabrication. *Journal of Photochemistry and Photobiology C Photochemistry Reviews*. 2012;**13**(1):28-54

[32] Klyukin D, Silvennoinen M, Krykova V, Svirko Y, Sidorov A, Nikonorov N. Fluorescent clusters in chloride photo-thermo-refractive glass by femtosecond laser bleaching of Ag nanoparticles. *Optics Express*. 2017;**25**(11):12944

[33] Ivanov SA, Nikonorov NV, Dubrovin VD, Krykova VA. Analysis of the hologram recording on the novel chloride photo-thermo-refractive glass. In: *Proceedings of SPIE. The International Society for Optical Engineering*; 2017

[34] Collier RJ, Burckhardt CB, Lin LH. Diffraction from volume holograms. In: *Optical Holography*. Amsterdam, Netherlands: Elsevier; 1971. pp. 228-264

[35] Fally M, Ellabban M, Drevenšek-Olenik I. Out-of-phase mixed holographic gratings: A qualitative analysis. *Optics Express*. 2008;**16**(9):6528